Self-diffusion and sedimentation of tracer spheres in (semi)dilute dispersions of rigid colloidal rods

Sebastiaan G. J. M. Kluijtmans,* Gijsberta H. Koenderink, and Albert P. Philipse†
Van't Hoff Laboratory for Physical and Colloid Chemistry, Debye Research Institute, Utrecht University, Padualaan 8, 3584 CH Utrecht, The Netherlands
(Received 8 July 1999)

Long-time self-diffusion and sedimentation of fluorescent tracer spheres in electrostatically stabilized dispersions of rigid colloidal host rods have been measured *in situ* with fluorescence recovery after photobleaching, and gravitational and ultracentrifugal sedimentation. The dynamics of silica tracer spheres of 39 and 370 nm radius was monitored in dispersions of host rods with aspect ratios 9.6 and 25.7 at various rod volume fractions. The translational and rotational diffusion coefficient of the host rods was obtained independently with dynamic light scattering and birefringence decay measurements. Our results indicate that sedimentation and long-time self-diffusion are determined by the same friction factor. Furthermore we find that, as long as the host rods are relatively mobile, tracer sphere sedimentation and long-time self-diffusion are governed by the macroscopic solution viscosity, regardless of the tracer and host rod size. However, when the host rods are immobilized, due to rod entanglements at higher volume fractions, tracer sphere dynamics depends strongly on the tracer size relative to the pore size of the host rod network. The large tracers are completely trapped in the network whereas the small tracer spheres remain mobile. Current models for tracer sphere motion in rod assemblies do not satisfactorily explain the complete dynamic regime covered by our experimental model system because the effect of host rod mobility is not properly taken into account.

PACS number(s): 66.30.Fq, 83.70.Hq, 82.70.Dd

I. INTRODUCTION

Diffusion of colloidal tracers in hindering media has often been studied for host solutions of polymers, focusing on the effect of polymer length, polymer concentration, and tracer size on the tracer dynamics. It is often found that tracer diffusion is governed by the effective macroscopic viscosity of the polymer solution, although in several cases deviations from this effective viscosity behavior are observed. Experimental work has focused on tracer dynamics in solutions of flexible polymers which exhibit diffusional and reptationlike motion. Comparison with various theoretical models for diffusion in polymer solutions is difficult, because these models nearly always assume the polymers to be immobile, rigid rods. Here we report on the dynamics of colloidal silica tracer spheres in a host dispersion of *rigid* colloidal rods, consisting of a crystalline boehmite core covered with a thin silica shell. In addition to the well-defined size and shape of the colloids, the silica host and tracer particles are negatively charged. This excludes attractions between host and tracer. To our knowledge, there is only one previous example of the use of rigid host rods, by Tracey and Pecora [1]. These authors used dynamic light scattering to measure tracer diffusion, whereas we use fluorescence recovery after photobleaching (FRAP) which allows us to probe a longer time scale.

Our primary aim is to investigate whether the effect of isotropically distributed rigid host rods on the dynamics of a single tracer sphere can be predicted by an effective viscosity in the sphere friction factor. In addition to tracer long-time self-diffusion we also measure tracer sedimentation. The few earlier publications that combine both measurements [2–4] are not conclusive on the question whether sedimentation and self-diffusion should yield the same tracer friction factor. It appears that agreement depends on the time scale for the dynamics monitored in the experiments [2–4].

In this paper we report long-time self-diffusion and sedimentation coefficients of monodisperse, fluorescent silica spheres for two largely different sphere sizes. Furthermore, we have used host dispersions of silica-coated boehmite rods with two different aspect ratios at rod concentrations varying from the dilute to semidilute regime. The dynamic behavior of the colloidal host rods themselves is monitored with various techniques (dynamic light scattering, birefringence decay after shear aligning, and low-shear viscosity measurements). The host rod dispersions cover a wide dynamic range, from mobile (dilute regime) to static (entangled rods). Consequently, tracer dynamics also covers a wide range of dynamic regimes, from tracer motion governed by the effective viscosity of the rod solution (dilute host dispersions) to tracer motion determined by the pore size distribution of an almost fixed network of rods (entangled host dispersions). This demonstrates that tracer mobility in hindering media is strongly coupled to the dynamics of the host particles, which is not adequately taken into account in current theoretical models for tracer motion in rod networks.

II. BACKGROUND

In this section we briefly recapitulate literature on theory and experiments on confined tracer motion in host dispersions. The Brownian motion of a single colloid is character-

*Present address: Fuji Photo Film, Tilburg Research Laboratory, Oudenstaart 1, P.O. Box 90156, 5000 LJ, Tilburg, The Netherlands.
†Author to whom correspondence should be addressed.

ized by its mean-squared displacement $\langle \Delta r^2 \rangle$, which on the diffusive time scale is a linear function of time:

$$\langle \Delta r^2(t) \rangle = 6 D_0 t. \tag{1}$$

The free-particle diffusion coefficient D_0 of a sphere with hydrodynamic radius R in a solvent with viscosity η_0 is given by the Stokes-Einstein equation:

$$D_0 = \frac{kT}{f_0} = \frac{kT}{6\pi\eta_0 R}. \tag{2}$$

Here k is the Boltzmann constant, T is the absolute temperature, and f_0 is the Stokes friction factor, which also determines the sedimentation coefficient s_0 of the free sphere via

$$s_0 = \frac{v(\rho - \rho_0)}{f_0} = \frac{2(\rho - \rho_0)R^2}{9\eta_0}, \tag{3}$$

where ρ and ρ_0 are the particle and solvent mass density and v the particle volume.

The presence of obstacles in the diffusion or sedimentation path of the tracer sphere will alter the above stated diffusion and sedimentation coefficients through direct and hydrodynamic interactions. Experimental results of tracer sphere diffusion and sedimentation in polymer solutions are usually compared to Eq. (2) and (3), replacing f_0 by a modified Stokes friction factor

$$f = 6\pi\eta(\varphi)R, \tag{4}$$

with φ being the volume fraction of the obstacles [1–19]. Equation (4) implies that the host dispersion is effectively replaced by a homogeneous fluid with viscosity $\eta(\varphi)$. Agreement with Eq. (4) is usually referred to as ''Stokes-Einstein behavior.'' This behavior implies for the long-time self diffusion coefficient D and sedimentation coefficient s of a tracer in a host dispersion: $D/D_0 = s/s_0 = \eta_0/\eta(\varphi)$.

For many experimental systems Stokes-Einstein behavior has been reported, especially for large tracers [1,5,7,12–14]. In some cases, however, a friction factor is observed, which is larger than expected from the solution viscosity. This is usually ascribed to polymer adsorption onto the probe particle or polymer-induced sphere aggregation [2,3,8,10,20,21]. On the other hand, smaller friction factors than predicted by Eq. (4) are frequently observed for tracers which are small in comparison to host particles [5–7,9–11,15,17,22–25]. These smaller friction factors are usually rationalized following Langevin and Rondolez [26], who modeled (semidilute) polymer solutions as a transient gel which is static on the time scale of tracer motion. For this gel one can define an average pore size or ''mesh size'' ξ. For large particles or high rod concentrations (for which $R/\xi > 1$) the polymer solution behaves like a homogeneous fluid, and the friction factor is determined by the macroscopic solution viscosity [Eq. (4)]. Tracers which are substantially smaller than the mesh size ($R/\xi < 1$) see a discontinuous environment and experience a local viscosity which is closer to the pure solvent viscosity (η_0) than to the macroscopic solution viscosity (η). In other words, small tracers will diffuse faster than expected on the basis of the macroscopic viscosity.

Apart from the effective viscosity approach expressed by Eq. (4), experimental data for tracer motion in polymer solutions are also frequently interpreted using the following stretched-exponential expression for f_0/f:

$$\frac{f_0}{f} = \exp(-\alpha c^{\nu}) \tag{5}$$

with c the polymer concentration in gram per liter, and ν and α fit parameters. Experimental results for the concentration exponent ν vary between 0.5 and 1. Generally good agreement with Eq. (5) is found for most of the diffusion and sedimentation data [1,2,4,7,13,15,17–19,21,22,24,25,27–31]. This is in itself not surprising, since Eq. (5) is a very flexible fitting function. Moreover, the polymer solution viscosity itself also follows a stretched exponential, though not always with the same values for ν and α [17–19]. The stretched-exponential form is also found in theoretical work on tracer motion in polymer solutions. This theoretical work assumes fixed host obstacles (see below), with the exception of Phillies' model for mobile hosts [32–36]. Phillies proposes that the retardation of spheres by a rod solution is analogous to sphere retardation by hydrodynamic interactions with a collection of other spheres, resulting in $\nu = aR^u M^x$, where M is the polymer molecular weight and a, u, and x are scaling parameters. This result is claimed to be valid for both dilute and (entangled) semidilute polymer solutions.

The assumption that tracers diffuse in polymer solutions which behave as static rod networks is reasonable for entangled polymers, which slowly fluctuate on a time scale much longer than the time scale of tracer motion. However, this description will probably break down for more dilute polymer solutions where polymers are relatively mobile. The first theoretical treatment of tracer motion in a static rod network is due to Ogston [37], who determined the geometric effect of immobile, rodlike obstacles (with thickness d) on tracer mobility. Ogston's final result for the reduced friction factor is

$$\frac{f_0}{f} = \exp\left(-\frac{R}{1/2d}\sqrt{\varphi}\right) \tag{6}$$

[note that Eq. (6) is equivalent to Eq. (5) when ν is equal to 0.5 and α proportional to R]. Ogston neglects hydrodynamic interactions. Nevertheless, results similar to Eq. (6) are found for purely hydrodynamic models. For instance, Cukier derived a stretched-exponential expression [38]:

$$\frac{f_0}{f} = \exp(-\kappa R) = \exp(-\varphi^{\mu} R) \tag{7}$$

with a concentration exponent μ which equals 0.5 for rodlike hosts and a prefactor proportional to R. The matrix-dependent screening constant κ depends on the resistance of the host rod network to fluid flow. For solutions of flexible polymer chains instead of rigid rodlike particles. Altenberger [39] showed that $0.5 < \mu < 1$, depending on polymer concentration and the strength of hydrodynamic interactions between polymers. Phillips *et al.*, [40,41] suggest an alternative hydrodynamic approach, modeling the fiber network (assumed immobile) as an effective Brinkman medium charac-

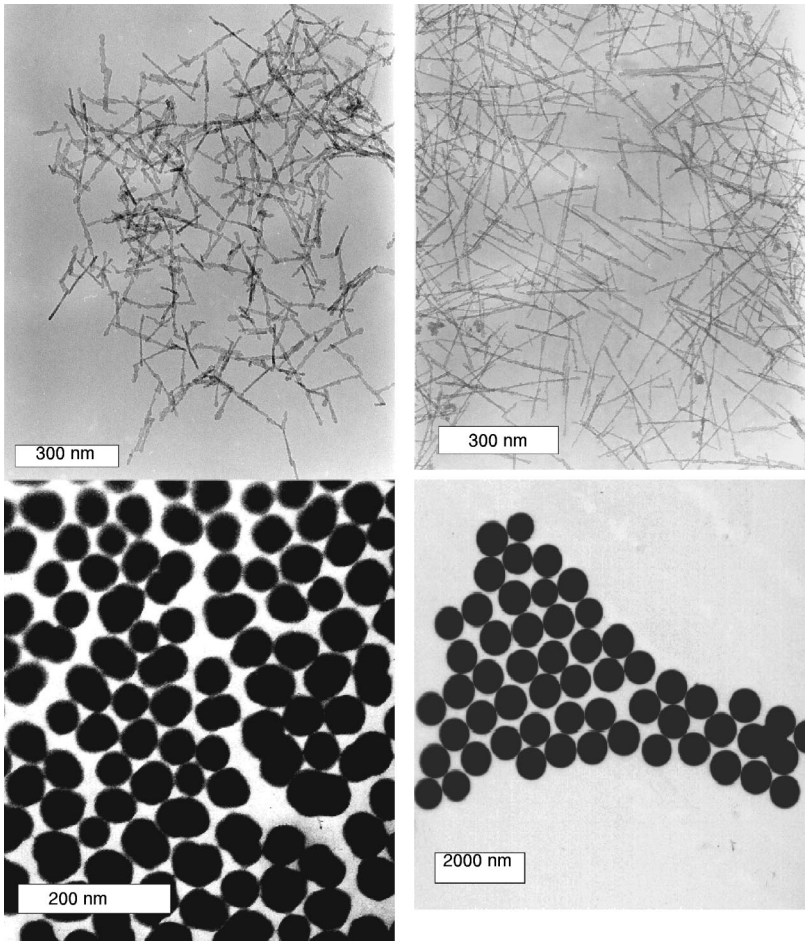

FIG. 1. TEM photographs of colloidal host rods (silica-coated boehmite rods $L100$ and $L200$), and the fluorescent silica tracer spheres $D78$ and $D740$. Particle dimensions are given in Tables I and II.

terized only by its hydraulic (Darcy) permeability. This approach has been shown to be equivalent to that of Cukier and Altenberger [6].

Clearly, current theoretical models do not yet completely incorporate the features of real tracer-host systems, like the host-particle dynamics. On the other hand, discrimination between various models with experiments is often difficult due to factors such as host-tracer attractions and host particle flexibility. This, among other things, is the motivation for developing rigid, (fluorescent) inorganic model colloids [42–44].

III. EXPERIMENT

A. Preparation and characterization of colloidal tracer spheres and host rods

Silica-boehmite rods

Silica-coated boehmite rods (hereafter silica rods) of two different aspect ratios (10 and 26) were used as host particles. The host rods were prepared in two steps. First, aqueous dispersions of boehmite (γ-AlOOH) rods were synthesized following Buining [42]. In the second step the boehmite needles are given the same surface as the silica tracers; the rods are coated with a thin layer of silica by titration with an aqueous solution of sodium silicate (''waterglass''), following Van Bruggen [43]. The host dispersions were coded $L100$ (length 102 nm) and $L200$ (length 229 nm). The rods were transferred to pure *N,N*-dimethylformamide (DMF) by repeated centrifugation and redispersion. To redisperse the rods, the solutions were shaken by hand and with a vortex mixer. (No ultrasonic treatment was applied because it may break the thin rods.) DMF is an excellent solvent to suspend silica colloids, probably because of a structured solvation layer of DMF molecules at the silica surface [45]. The final stock solutions contained $0.7\% v/v (\approx 20\,\mathrm{g/l})$ rods. Representative electron micrographs of the two host rod systems are shown in Fig. 1, from which the average particle dimensions and size polydispersity were determined (see Table I).

Fluorescent silica spheres

Silica spheres with a hydrodynamic diameter of 78 and 740 nm were used as tracer particles. The two systems were coded D78 and D740, respectively. The silica spheres were prepared following Stöber *et al.* [46], and labeled with the fluorescent dye fluorescein isothiocyanate (FITC) following Van Blaaderen [44]. The spheres were dispersed in a solution

TABLE I. Number average length (L) and diameter (D) of $L100$ and $L200$ silica-boehmite rods, determined by digital image analysis of electron micrograps.

System code	L (nm)	D (nm)	L/D
$L100$	101.9 ± 39.7	10.6 ± 3.3	9.6
$L200$	228.9 ± 88.9	8.9 ± 2.0	25.7

TABLE II. Radius of silica tracer spheres, determined from electron micrographs (R_{TEM}) and from dynamic light-scattering experiments (R_{DLS}).

System code	R_{TEM} (nm)	R_{DLS} (nm)
*D*78	32±3	39±1
*D*740	344±33	370±8

of 0.01*M* LiCl in DMF. For details on such dispersions see [44]. The sphere sizes were determined by digital image analysis of transmission electron micrographs (Fig. 1 and Table II). Hydrodynamic radii were measured with dynamic light scattering (DLS) on dilute samples in DMF (0.01*M* LiCl) at 25.0 °C using the 647.1 nm line from a Krypton laser (Spectra Physics model 2020).

Preparation of sphere-rod mixtures

Sphere-rod mixtures were prepared by addition of a small volume of concentrated stock dispersion of spheres in DMF to rod dispersions with rod volume fractions between 0 and 0.7 %. The final sphere volume fraction was ~1%, while the final salt concentration was fixed at 1 m*M* LiCl. Mixtures of silica-boehmite rods and silica spheres did not flocculate or gel over periods of at least 3 months. This is in marked contrast to mixtures of uncoated boehmite rods and silica spheres, which instantaneously and irreversibly gel as soon as the particles are mixed.

B. Dynamics of silica-boehmite rod dispersions

Low-shear viscosity and birefringence decay measurements

The low-shear viscosity of *L*100 and *L*200 rod dispersions in DMF (1m*M* LiCl) was measured using a Contraves Low Shear 40 rheometer equipped with a DIN406 Couette geometry, thermostatted at 25 °C. This geometry consists of two concentric cylinders with outer radius 3.25 mm and gap 0.25 mm. Viscosities were determined from the slope of shear stress versus shear rate plots. Relative viscosities were obtained by dividing the viscosities of the rod dispersions by the solvent viscosity ($\eta_{DMF}=0.796$ mPas), which was determined under the same conditions. Dispersions of *L*100 rods were free-flowing (showing no visible yield stress) below $\varphi=0.007$. Dispersions of *L*200 rods were much more viscous. Above $\varphi=0.003$ *L*200 dispersions became gel-like, i.e., having a visible yield stress upon tilting.

The volume fraction dependence of the low-shear viscosity of a dispersion of rods is closely related to the volume fraction dependence of the rotational diffusion coefficient D_R of the rods, according to $\eta \approx \eta_0 + A\phi kT/D_{R,0} + B\phi kT/D_R$ (with *A* and *B* constants) [47–49]. Therefore, in case of the gel-like *L*200 dispersions, for which the (low-shear) viscosity could not be determined, the rotational dynamics ($0.0039<\varphi<0.007$) was examined instead. Rotational diffusion was measured using the optical birefringence setup described by Wierenga [50]. This setup comprises a transparent Couette geometry with a gap of 0.3 mm, in which a shear field can be applied by rotating the inner cylinder. The rods align in this shear field, giving rise to an optical birefringence signal Δn_{ss} [50]. In our experiments the shear field was switched off after 10 s and the decay of the birefringence $\Delta n(t)$, due to rotational Brownian motion, was monitored as a function of time *t*. The rotational relaxation time $t_R(\equiv 1/6D_R)$ of the rods was determined from the decay curves using $\Delta n(t)/\Delta n_{ss} = \exp(-t/\tau_R)$.

Dynamic light scattering

The translational diffusion coefficient of the silica host rods was determined with dynamic light scattering (DLS) at 25 °C using an argon laser source (Spectra Physics model 2000) operated at 250 mW power and a wavelength $\lambda = 514.5$ nm. Volume fractions of the *L*100 rods varied between $\varphi = 7\times10^{-4}$ and 6×10^{-3}. For the long *L*200 rods the range was $\varphi = 2\times10^{-4}$ and 4.3×10^{-3}. Intensity autocorrelation functions were obtained at six scattering angles (θ) between 30 ° and 120 °. The correlation functions were accumulated by a Malvern 7032 CE, 128 channel correlator up to 2×10^7 counts. The normalized intensity autocorrelation functions $g_1(K,t)$ were fitted to the second-order cumulant expression $g_1(K,t) = \alpha + \beta \exp\{-b(K)t + c(K)t^2\}$, where *K* is the wave vector given by $K = 4\pi n/\lambda \sin(\theta/2)$, *t* is time and α, β, $b(K)$, and $c(K)$ are fit parameters. For noninteracting rods, i.e., at low concentrations, we found that this cumulant fit describes the full decay of the correlation function, while at high concentrations it only describes the initial slope of the correlation function. The translational diffusion coefficient (D_T) is related to the decay exponent $b(K) = 2K^2 D_T$ (valid for rods with $KL<5$ [16]). D_T was determined from the slope of $b(K)$ versus K^2 plots by a linear least-squares fit.

C. Dynamics of silica tracer spheres in rod dispersions

Fluorescence recovery after photobleaching

The long-time self-diffusion coefficient of tracer spheres in host rod dispersions was determined using fluorescence recovery after photobleaching (FRAP). Details of the experimental setup and theory of the FRAP technique can be found for example, in [45,51]. In short, a sinusoidal fringe pattern is created in the sample by crossing two high intensity coherent laser beams under an angle 2θ for a short period of time. The wave vector of the fringes is $k = (4\pi/\lambda)\sin\theta$, where λ is the wavelength of the laser light. During the short pulse (typically 1 s), part of the fluorescent dye in the tracer particles is irreversibly decomposed, leaving a sinusoidal fluorescence profile complementary to the fringe pattern of the crossed laser beams. The gradual decay of the fluorescence pattern as a result of the diffusive exchange of bleached and unbleached particles is monitored using a low-intensity reading laser beam. For monodisperse Brownian particles the fluorescence signal $S(k,t)$ decays exponentially in time (t) according to $S(k,t) = a + b\exp(-D_S^L k^2 t)$ [52], where D_S^L is the long-time self-diffusion coefficient of the tracer particles and *a* and *b* are constants. Since *k* values are usually small, diffusion is probed over large distances. In our experiments we used $k = 3\times10^5\ \mathrm{m}^{-1}$ for the small spheres and $k = 6\times10^5\ \mathrm{m}^{-1}$ for the large spheres, corresponding to diffusion distances of 21 and 10 μm, respectively. These distances are much larger than those probed by dynamic light scattering, which are at most a few microns.

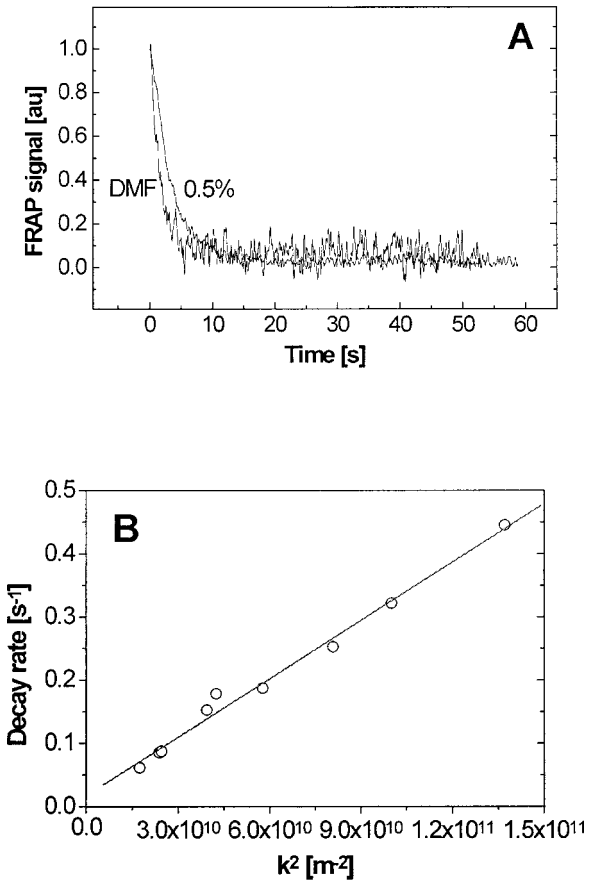

FIG. 2. (a) Typical FRAP curve normalized on the signal at $t=0$ s, obtained for a $D78/L100$ mixture with $\varphi_{\text{sphere}}=1.0\%$ and $\varphi_{\text{rod}}=0.5\%$ at $k^2=1.0\times10^{11}\,\text{m}^{-2}$. (b) Decay rate as a function of the squared wave vector k^2. The drawn line is a linear fit with a slope $D_{S.L}=3.08\times10^{-12}\,\text{m}^2/\text{s}$.

For bleaching and excitation of the fluorescent dye inside the particles, the 488 nm line of an argon laser (Spectra Physics series 2000) was used. Bleaching patterns were created using a light pulse of 500 ms at 250 mW for the $D740$ spheres, and 1000 ms at 400 mW for the $D78$ spheres. During monitoring of the decay of the bleach pattern, the laser intensity was reduced by a factor of 500 to 1000. Rod-sphere mixtures were transferred to glass cuvettes (Vitro Dynamics) with dimensions 0.4×5 mm/(for the D78 spheres) or 0.17×2 mm (for the D740 spheres). Samples were allowed to equilibrate for at least 30 min before starting the FRAP experiments. For each sample, between 10 and 20 FRAP curves were recorded at different positions in the cuvette. These curves were averaged and fit to a monoexponential decay. A typical FRAP curve is shown in Fig. 2. The resulting D_L was normalized on D_0, which is the diffusion coefficient of the tracers measured at the same tracer concentration in the absence of rods. All FRAP measurements were conducted at 23 °C.

Sedimentation of silica tracer spheres in host rod dispersions

Sedimentation experiments of the large silica tracers (D740) in host rod dispersions were carried out by gravitational settling in a setup carefully thermostatted at 21.5 °C as described by Thies-Weesie [53]. The height of the interface between the settling sphere-containing dispersion and sphere-free dispersion was measured as a function of time. Due to the monodispersity of the spheres (and their slow diffusion) the sedimentation boundary was very sharp and, therefore, easy to determine. The sedimentation velocity follows from the slope of height versus time plots. After each experiment samples were homogenized by shaking and a duplo experiment was performed. Experiments were highly reproducible. Since the sedimentation technique is very sensitive to aggregation and even slight attractions [53], the reproducibility of the measurements shows that the rods and spheres do not aggregate, not even in the sediment which is compressed by gravity.

To sediment the small D78 spheres, which do not settle significantly under gravity, an analytical ultracentrifuge (Beckman XI, 3500 rpm, 25.0 °C) was used. The initial sphere concentration was fixed at 0.5% (v/v). Concentration distributions of the sedimenting tracer particles were followed during 30 min with a photoelectric scan system, using the characteristic absorption of FITC at 498 nm. The host rods do not absorb this wavelength so the scan only detects the sedimenting tracer spheres. The sedimentation coefficient s follows from $\ln(r_b/r_m)=s\omega^2t$, with r_b being the radial position of the sedimentation boundary, r_m the position of the meniscus, ω the radial velocity, and t the time. In the first scans after the start of each sedimentation run we observed the appearance of a sharp peak at the sedimenting boundary. Dogic *et al.* [54] observed the same effect for (concentrated) dispersions of *fd*-virus rods, and explained it as an artifact of the detection system, namely the refraction of light at the steep gradient in refractive index at the sedimenting boundary. Neither in Ref. [54] nor in this work does the peak interfere with the determination of the sedimentation boundary.

IV. RESULTS

A. Rod dynamics

Low-shear rheology of rod dispersions

Low-shear viscosities of dispersions of short ($L100$) and long ($L200$) rods were obtained from shear stress versus shear rate flow curves measured between 0.01 and 50 s^{-1}. In the concentration range studied (up to 0.7 vol %), dispersions of short rods showed Newtonian behavior. In addition, no hysteresis was present between flow curves with increasing and decreasing shear rates. For dispersions of long rods, Newtonian behavior was only observed for very small volume fractions up to 0.03%. At higher volume fractions, dispersions were shear thinning with considerable hysteresis between the downward and upward shear rate sweeps. Apparently, the rotational dynamics of the rods are restricted to such an extent, that they align in the applied shear flow.

For both rod systems, relative viscosities η_r were obtained from the slope of the linear (part of the) flow curves. The viscosity as a function of the rod volume fraction is shown in Fig. 3. For the short rods the relative viscosity ranges from 1.1 at 0.06% rods to 2.7 at 0.6%. All dispersions of short rods are free-flowing. Much higher viscosities were obtained for dispersions of long rods. Above 0.1% rods the relative viscosity strongly increases and above 0.3% the

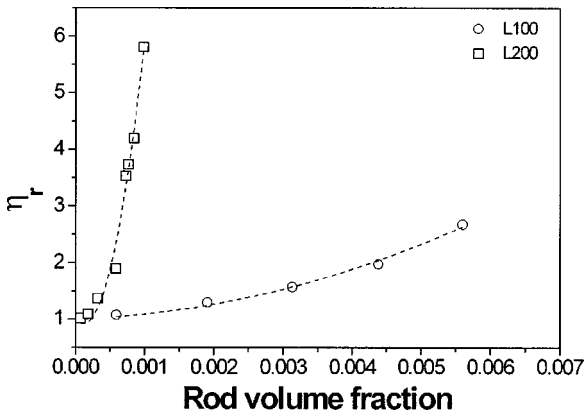

FIG. 3. Relative low shear viscosity of dispersions of short rods ($L100$) and long rods ($L200$) in DMF (1 mM LiCl) as a function of the rod volume fraction. The drawn curves are fits to Eq. (8).

samples are gel-like and do not readily flow upon tilting the dispersion by 180°. For both rod systems the viscosity results were fit to

$$\eta_r = 1 + [\eta]\varphi + C_2\varphi^2, \tag{8}$$

where $[\eta]$ is the intrinsic viscosity and $C_2 = [\eta]^2 k_H$, with k_H the Huggins coefficient [50]. For the short rods a reasonable fit is obtained (see Fig. 3), resulting in $[\eta] = 46$ and $k_H = 20$. Alternative values for $[\eta]$ and k_H can be determined by linear regression of the specific viscosity $[(\eta_r - 1)/\varphi]$ as a function of the rod concentration, yielding $[\eta] = 88$ and $k_H = 4$. The latter values do not agree with the values obtained by fitting the relative viscosity, which is probably due to the small number of data points that was available. It is clear, anyhow, that the experimental values of the intrinsic viscosity and Huggins coefficient are considerably larger than predicted by theories for noninteracting hard rods ($[\eta] = 12$ and $k_H = 0.4$ [55,56]).

The viscosity data of the large $L200$ rods are not well represented by Eq. (8) (see Fig. 3). Unphysical negative values of $[\eta]$ are obtained. However, for these long rods, volume fractions of 0.1% are already close to the semidilute regime where Eq. (8) can no longer be applied [50]. (The onset of the semidilute regime can be estimated by $\varphi^* = (d/L)^2$, which for the $L200$ is equal to 0.15%.)

The large discrepancy between experiments and theory is probably due to the presence of other than hard rod interactions, such as double layer repulsion or van der Waals attraction. However, no signs of attraction were observed in our systems, neither in unsheared nor in sheared dispersions of $L100$ and $L200$ rods. The dispersions were stored for 3 months without changing their appearance. The birefringence decay measurements of $L200$ rods (see next section) show that the rotational dynamics of the rods become faster with increasing salt concentration, which is characteristic for dispersions in which double layer repulsion dominates the interparticle interactions [50]. For a system of attractive rods, salt addition would lead to irreversible flocculation, and hence slower dynamics.

Rotational diffusion of long ($L200$) rods

Rotational dynamics of the long $L200$ rods was studied by measuring the relaxation of the optical birefringence of dispersions after cessation of an applied shear flow. As shown in Fig. 4(a) the relaxation times strongly depend on the salt concentration. At low ionic strengths, rotational dynamics is ten times slower than at the highest salt concentration. Apparently, the rotational dynamics of these charged silica-boehmite rods are strongly influenced by double-layer interactions, which become increasingly important at low ionic strength. At 1 mM LiCl the relaxation time was of the order of 0.34 s, which is a factor of 2000 larger than predicted for infinitely dilute hard rods with aspect ratio 25.7 [55]. Evidently, the rotational mobility of the rods is strongly hindered at these rod and salt concentrations.

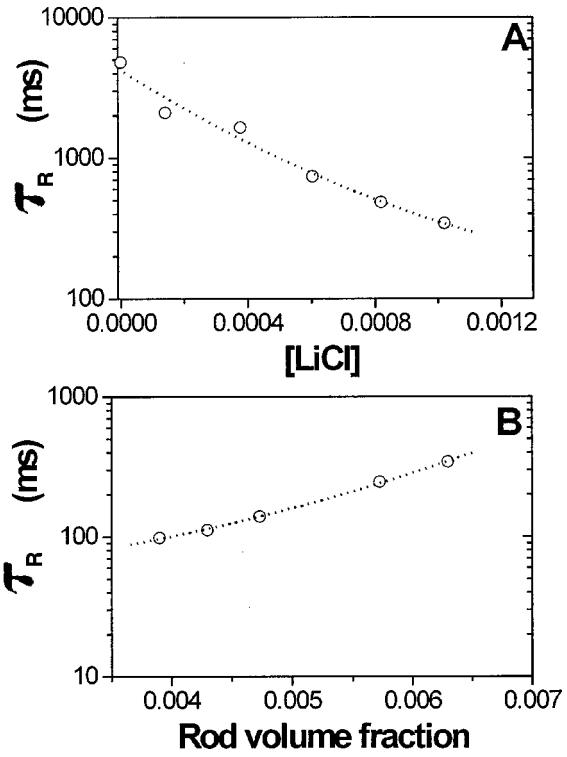

FIG. 4. Rotational relaxation times τ_R for $L200$ host rods in DMF (0.7%) (a) as a function of the added LiCl concentration; shear rate 94 s^{-1}. The relaxation times are strongly affected by the ionic strength. (b) as a function of rod concentration at initial shear rate of 94 s^{-1}. The relaxation times decrease with decreasing rod concentration. Dotted lines are to guide the eye.

The salt concentration was now fixed at 1 mM LiCl and the rod volume fraction was decreased stepwise to 0.39%. (Lower volume fractions cannot be attained because of the small birefringence signal.) Figure 4(b) shows the measured relaxation times as a function of rod concentration. Although the relaxation time decreases by a factor of 3.5 on going from 0.7% rods to 0.39% ($\tau_R = 0.098$ s) it is still 600 times slower than the relaxation of a single hard rod.

Translational diffusion of host rods

The translational motion of short and long rods in DMF (1 mM LiCl) was measured using dynamic light scattering. Scattering vectors (K) were chosen such that $KL < 5$, so that rod rotation did not significantly affect the DLS autocorrelation functions [16]. Correlation functions of the $L100$ systems were well represented by a single exponential decay for volume fractions up to 0.3%. (Generally, a second-order

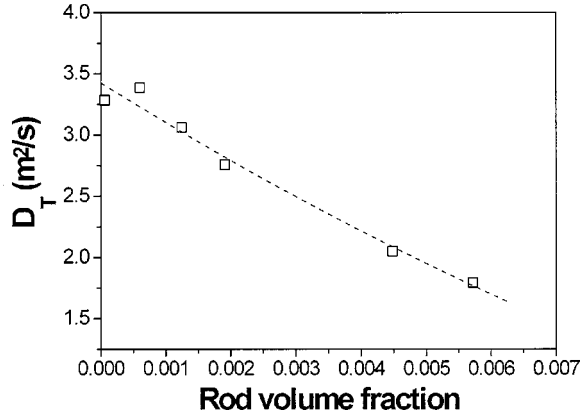

FIG. 5. Translational diffusion coefficients (D_T) of short ($L100$) silica-boehmite rods in DMF (1 mM LiCl), obtained with DLS for various rod concentrations. Data are obtained from plots of K^2D_T versus K^2. The dotted line is to guide the eye.

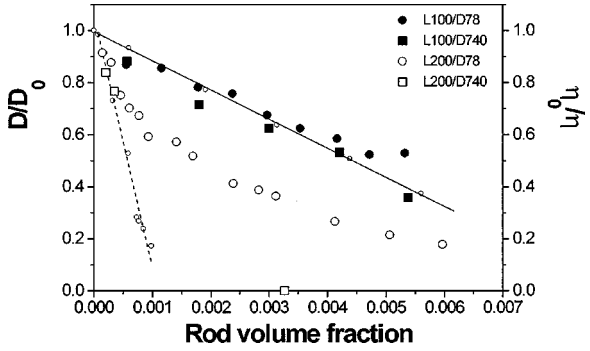

FIG. 6. Reduced diffusion coefficients of the $D78$ and $D740$ silica tracer spheres in dispersions of $L100$ and $L200$ rods; $D_{0,D78}=6.01\times10^{-12}\,\mathrm{m^2/s}$, $D_{0,D740}=0.70\times10^{-12}\,\mathrm{m^2/s}$. The drawn and dashed lines represent linear fits to the inverse relative viscosities of, respectively, the $L100$ and $L200$ rod dispersions (small dots).

cumulant was included to account for polydispersity effects.) At volume fractions above 0.3%, correlation functions became multiexponential and decay rates were extracted from the initial decay of the correlation function. At all concentrations studied the decay rate slightly decreases with decreasing wave vector. This is probably due to the size polydispersity of the rods of ~40%. At each volume fraction, diffusion coefficients D_T were extracted by linear fits of K^2D_T versus K^2. In Fig. 5, the $L100$ diffusion coefficients thus obtained, are plotted as a function of rod volume fraction. The rod mobility decreases considerably with increasing rod concentration. Extrapolation to $\varphi=0$ yields $D_\tau=3.5\times10^{-12}\,\mathrm{m^2/s}$, which is a factor of 4 slower than predicted by Tirado *et al.* [57] ($D_0=1.4\times10^{-11}\,\mathrm{m^2/s}$).

For the $L200$ rods no single-exponential correlation functions were observed even for rod volume fractions as low as 0.02%. At volume fractions of 0.4% and higher DLS curves were nonergodic, indicating spatial confinement of the rods on the DLS time scale. At $\varphi=0.02\%$ we estimate $D_T=2\times10^{-12}\,\mathrm{m^2/s}$, which is again five times smaller than theoretically predicted.

There is yet no satisfactory explanation for the discrepancies between theoretical and experimental diffusivities of single rods. Similar discrepancies are reported for dilute aqueous dispersions of boehmite rods [50] and silica-coated boehmite rods [58].

B. Self-diffusion of tracer spheres in host rod dispersions

Self-diffusion coefficients of the fluorescent $D78$ and $D740$ tracer spheres as a function of the rod volume fraction are shown in Fig. 6. In general, the diffusion of both small and large tracers is strongly restricted by the presence of rods. Significant sphere retardation already appears at rod volume fractions as small as 0.1%, especially in $L200$ dispersions. If we compare this with the retardation of tracer spheres in dispersions of host spheres, where 50% retardation is observed at host volume fractions of 10% [45], it is clear that rods are much more effective in hindering particle motion.

The $D740/L200$ mixtures in FRAP cuvettes at $\phi>0.05\%$ showed an unexpected phase behavior (which was not observed in sedimentation tubes). FRAP measurements on these samples were not reproducible over time periods of several hours, in contrast to other samples, which were stable within 15 min. At rod concentrations larger than 0.3% the samples became visibly inhomogeneous. In some samples Bragg reflections were observed after several hours, indicating the formation of crystalline regions of spheres. These observations of phase separation in a rod-sphere system are described in detail elsewhere [59].

In Fig. 6 the diffusion coefficients are also compared to the inverse relative viscosity of the rod host dispersions in the absence of tracers. In case Eq. (4) applies, the diffusion data should coincide with the inverse solution viscosity. For the small $L100$ rods this is indeed the case. The reduced diffusion coefficients quite accurately follow the inverse viscosity, although the reduced diffusion coefficients of the small tracers tend to be somewhat larger than for the large tracers. The latter effect is visible especially at high rod concentrations, where a small upward deviation is observed for the $D78$ spheres. This point may be the onset where the host rods become relatively immobile and geometric effects become important. For the long $L200$ rods the deviation from the inverse viscosity already sets in at much lower rod concentrations of 0.03%. At higher volume fractions the diffusion of the small tracers is much faster than expected from the solution viscosity. Deviations from Eq. (4) are visualized more clearly in Fig. 7 where $\eta D/\eta_0 D_0$ is plotted as a function of the rod volume fraction. If Eq. (4) applies, $\eta D/\eta_0 D_0$ equals unity. For the $D78$ spheres in $L200$ dispersions $\eta D/\eta_0 D_0$ almost immediately starts to increase and deviate from Eq. (4). For the $D740/L200$ system no firm conclusions regarding Stokes-Einstein behavior can be drawn. Only two data points could be obtained because of the unexpected phase separation phenomena for $\phi>0.05\%$.

C. Sedimentation of tracer spheres

Sedimentation coefficients of $D78$ and $D740$ tracer spheres in dispersions of silica-boehmite rods $L100$ and $L200$ are collected in Fig. 8 as a function of the rod volume fraction. Sedimentation experiments were performed either with an analytical ultracentrifuge for $D78$ spheres at a sphere volume fraction of 0.5% or under gravity for $D740$ spheres at a sphere volume fraction of 1%. Data were normalized by

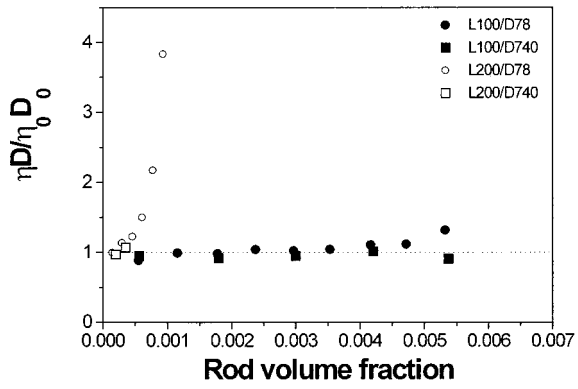

FIG. 7. Product of the tracer sphere diffusion coefficient, normalized by its value at infinite dilution, and the relative viscosity of the host rod dispersion. The dashed line corresponds to the generalized Stokes-Einstein equation.

the sedimentation coefficient measured at equal sphere concentration but in the absence of rods. In this way, the influence of sphere-sphere interactions, if any, is removed from the experimental data.

The following calculation shows that in all our experiments sphere sedimentation is monitored through an assembly of nonsedimenting rods. Using the friction factor of a single sphere [see Eq. (2)] and a single rod (as given by Tirado [57]) we find $s_{L200}=632$ S and $s_{L100}=606$ S for the $L200$ and $L100$ rods, and $s_{D78}=4774$ S and $s_{D740}=378\,000$ S for the $D78$ and $D740$ spheres. Compared to the large tracers the rods do not sediment significantly, but even the small tracers should sediment about eight times faster than the rods. At finite volume fractions the difference will be even larger since the sedimentation of the rods has a much stronger volume fraction dependence than that of spheres.

The sedimentation results presented in Fig. 8 very much resemble the diffusion data in Fig. 6. Like diffusion, sphere sedimentation is strongly hindered by the presence of rods. Again we find that in dispersions of $L100$ rods the sedimentation coefficient of both tracer spheres closely follows the inverse viscosity. Hence, the viscosity increase with increasing rod concentration can fully account for the reduction of

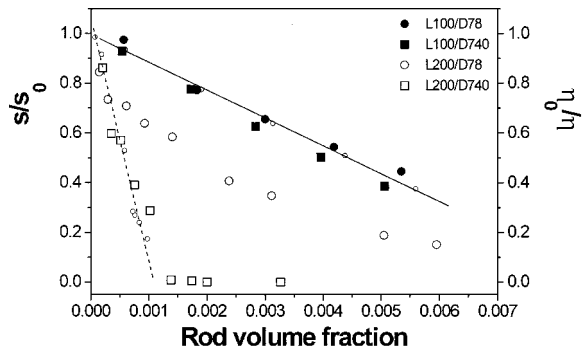

FIG. 8. Reduced sedimentation (s/s_0) coefficients for $D78$ and $D740$ silica tracer spheres in dispersions of $L100$ and $L200$ host rods as a function of rod concentration. Sedimentation rates of the small tracers in $L200$ dispersions are higher than the inverse relative viscosity. Other sedimentation data coincide with the Stokes-Einstein prediction. For $\varphi \geqslant 0.2\%$, sedimentation of the $D740$ spheres in $L200$ dispersions is arrested.

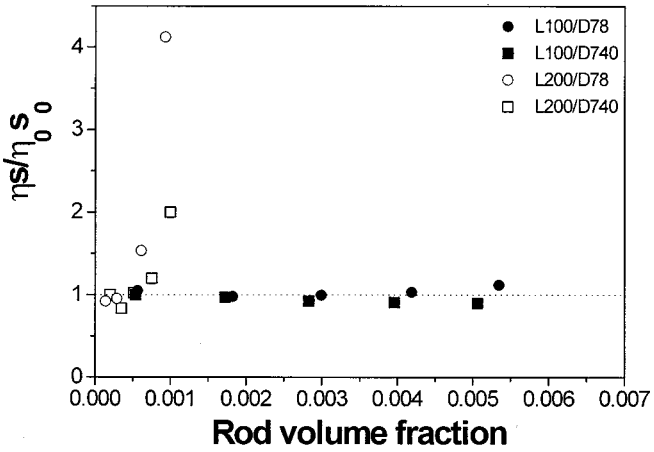

FIG. 9. Product of the sedimentation diffusion coefficient, normalized by its value at infinite dilution, and the relative viscosity of the host rod dispersion for all four combinations of spheres and rods. The dashed line corresponds to the generalized sedimentation equation.

the sedimentation rate. Also sedimentation of large $D740$ spheres in $L200$ dispersions coincides with the inverse viscosity at low volume fractions, although at the highest volume fraction near complete immobilization ($\phi \approx 0.001$) the sedimentation rate is somewhat faster. For $\phi > 0.001$ no settling is observed even after several days. Here the large tracers are completely trapped by the rod network, whereas the small spheres remain mobile at least to $\phi = 0.6\%$. These findings are in agreement with recent calculations of Philipse and Kluijtmans [60] for the caging densities for spheres in static rod assemblies, which predict that the large spheres should be immobilized in the rod network at all experimental volume fractions. These calculations, incidentally, indicate that the large tracers should also be trapped in the $L100$ network if the $L100$ rods would have been static. Clearly this is not observed in our experimental systems, due to the mobility of the rods.

Although the small tracers are also hindered by the rods, they sediment much faster than expected from the dispersion viscosity. This can be clearly seen in Fig. 9 (similar to Fig. 7). For the $L200$-$D78$ system the product $\eta s/\eta_0 s_0$ again significantly deviates from unity. Note that also the $L100$-$D78$ system again shows the small, but significant, upward deviation at the highest experimental volume fractions. Probably this is the same onset of deviation from the macroscopic solution viscosity approach as observed in Fig. 7.

V. DISCUSSION

The main goal of this study is to investigate whether the effect of isotropically distributed rigid host rods on the dynamics of a single tracer sphere can be predicted by an effective viscosity in the sphere friction factor. As shown in Secs. IV B and IV C, we find diffusion and sedimentation friction factors, which are in accordance with the macroscopic solution viscosity for the large ($D740$) tracers irrespective of the host rod length. These observations confirm previous investigations of tracer dynamics in polymer solutions, which generally indicate agreement with Eq. (4) for relatively large tracer spheres [9,12,14,17,25,61]. In contrast,

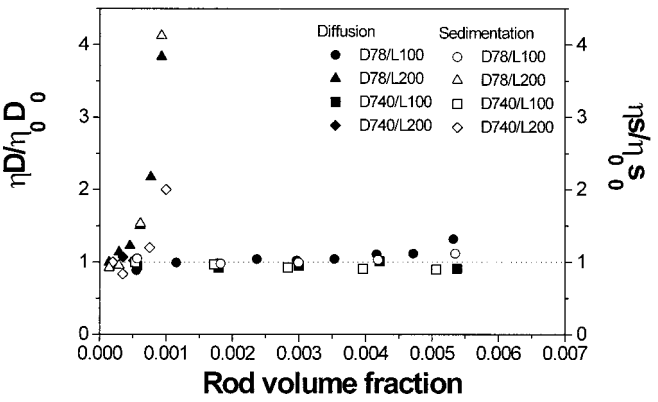

FIG. 10. Comparison of sedimentation (open symbols) and self-diffusion (filled symbols) of $D78$ and $D740$ silica spheres in $L100$ and $L200$ rod dispersions.

for the small $D78$ tracers agreement with Eq. (4) does depend on the rod length. Tracer dynamics in dispersions of short $L100$ rods is completely in accordance with Eq. (4), while for long $L200$ rods tracer sphere dynamics is considerably faster than predicted by the solution viscosity. In all cases, diffusion and sedimentation friction factors are equal within experimental error (see Fig. 10). Apparently, the tracer always probes a representative, macroscopic dispersion volume, such that the effective friction factor is the same.

Agreement or disagreement with the effective viscosity approach is often rationalized using the model of Langevin and Rondolez [6,11,12,15,17,24,25], which treats the host rod medium as a static network (on the time scale of tracer motion) with an average pore size ξ. Large tracers ($R>\xi$) will see a continuous fluid with viscosity $\eta(\varphi)$, while small tracers ($R<\xi$) experience a much smaller microviscosity which is close to η_0. For the large $D740$ spheres the Langevin and Rondelez approach explains our results. However, their approach does not explain why $D78$ tracers follow Stokes-Einstein behavior in $L100$ dispersions but not in $L200$ dispersions. The mesh size for $L100$ and $L200$ rods is very similar (ξ can be estimated by the cubic root of the number density). This suggests that modeling the rod medium as a static assembly on the time scale of tracer motion is not always appropriate.

To account for the different dynamic behavior of $D78$ tracers in $L100$ and $L200$ dispersions, respectively, we compare the relative motion of tracers and rods in both dispersions. At very low rod volume fractions experimental diffusivities are in the order of $10^{-11}\,\mathrm{m}^2/\mathrm{s}$ for both rod types and for the small tracer. The large tracer diffusivity is about ten times smaller. For the $L100$ rod systems, the rod diffusion coefficient is comparable to the diffusion coefficient of the tracers up to at least $\varphi_r=0.6\%$ (the highest experimental volume fraction). This implies that the tracer spheres experience a dynamic, continuously fluctuating, rod collection at all experimental rod volume fractions. For the $L200$ rods, at very low rod volume fractions ($\varphi_r=0.02\%$) the translational diffusion coefficient of tracers and rods is of the same order. At larger rod volume fractions diffusion coefficients could not be determined because DLS correlation functions were nonexponential. To estimate the rod mobility at higher volume fractions, other techniques were applied. The rotational motion of the $L200$ dispersions was measured using birefringence decay. The rotational diffusion coefficient of the $L200$ rods at $\varphi_r=0.39\%$ is about a thousand times less than that of a single free rod (Sec. IV A), confirming the strongly restrained rotational motion of these rods which should also show up in viscosity results [47]. In Sec. IV A we reported that the viscosity of the $L200$ rods indeed steeply rises at volume fractions as low as $\varphi_r=0.1\%$. Hence, for $\varphi_r>0.1\%$ rotation of $L200$ rods is strongly constrained and these dispersions may be regarded as static networks on the diffusion time scale of a tracer sphere. As shown in Fig. 3, the viscosity rise for the $L100$ dispersions sets in only at the largest experimental volume fractions used (0.6%). Therefore, also from the point of view of rotational diffusion, these $L100$ dispersions should be regarded as dynamic networks. Interestingly, these findings comply with the minimum overlap concentration estimated from $\phi^*\cong(D/L)^2$, where ϕ^* is the minimum volume fraction of rods where permanent overlap of rotational volumes occurs. For concentrations $\phi>\phi^*$ interparticle interactions start to play a dominant role on dispersion properties like rotational diffusion and, related to it, viscosity [47]. For the $L200$ rods we find $\varphi^*=0.12\%$, which agrees quite well with the viscosity data. For the $L100$ rods, φ^* equals 0.7%. Therefore, the steep viscosity rise for the $L100$ rods is expected just outside the experimental range of volume fractions, which again complies with the viscosity results.

On the basis of this qualitative comparison between tracer and host dynamics, it is clear that for a dynamic rod network (such as the $L100$ dispersions), the concept of a static mesh size is only appropriate on time and spatial scales much shorter than the typical diffusion time and distance τ_r of the rods. On time scales larger than τ_r, which is the case in all our experiments, the dynamic $L100$ rod network fluctuates continuously due to translational and rotational diffusion of rods. So, although the small spheres in $L100$ dispersions are smaller than the average mesh size, they still have enough encounters with rods to probe the macroscopic viscosity. When on the other hand the rod network is static on the tracer time scale, like in case of the $L200$ dispersions, one should apply models for diffusion in static rod networks [37,38]. The model of Langevin and Rondelez [26], which discriminates between situations where the effective viscosity approach [Eq. (4)] does or does not apply, does not take into account the dynamic behavior of the host rods. It is important not only to consider the ratio between tracer and pore size, but also the relative mobility of tracer and host particles within the time frame of the experiment.

As argued above, $L200$ dispersions with rod volume fractions larger than 0.1% are expected to behave as static rod networks. Theoretical models for diffusion in static rod networks (see Sec. II) predict that tracer dynamics primarily depends on the tracer size relative to the average pore size (which is mainly controlled by the rod concentration). The majority of the available experimental data for tracer dynamics in semidilute polymer solutions and gels are fitted to a stretched exponential, which can represent either one of the models mentioned in Sec. II. We can fit all our data for the semidilute $L78$-$L200$ system very well with a stretched exponential, to obtain a concentration exponent ν of 0.76 for s/s_0 and 0.69 for D/D_0. These values are well within the

range of 0.5–1 predicted by theory [26,37–39,62] and similar to experimental values reported by others [1,2,4,7,13,15,17–19,21,22,24,25,27–31]. However, it should be noted that the stretched exponential is a rather flexible fitting function. Even the s/s_0 and D/D_0 data obtained for dynamic $L100$ dispersions can be fitted smoothly, taking $\nu = 1$ and α a constant independent of sphere size.

VI. CONCLUSIONS

We have investigated long-time self-diffusion of monodisperse fluorescent silica tracer spheres in dispersions of rigid silica-boehmite rods of known viscosity for various sphere and rod dimensions. These stable sphere-rod mixtures appear to be very suitable for a study of the tracer dynamics. Long-time tracer dynamics can be monitored *in situ* using FRAP and sedimentation.

Our main findings are that, under all experimental conditions here explored, the friction factors for long-time self-diffusion and sedimentation of tracers in rod dispersions are equal. Furthermore, we find that, as long as the host rods are mobile on the time scale of tracer sphere motion, the friction factor of the tracer spheres accurately follows the measured effective solution viscosity of the rod medium, regardless of the dimensions of the tracer spheres and host rods. The rod dispersion appears as a homogeneous viscous fluid to the tracer particle. On the other hand, when the host rods are immobilized due to strong entanglements at high volume fraction, the friction factor of the tracers can no longer be described using the solution viscosity. Instead, the mobility of the tracers is primarily determined by their size: tracers smaller than the typical pore size of the rod network are still mobile, whereas large tracers are trapped in the network, which behaves as a static porous medium. From these findings we conclude that the dynamics of tracer spheres in dispersions of host rods markedly depends on the mobility of the host rods. This mobility strongly decreases with increasing rod volume fraction and increasing aspect ratio. Current theoretical models do not properly take this effect of host rod dynamics into account.

ACKNOWLEDGMENTS

Professor H. N. W. Lekkerkerker is thanked for valuable discussions and remarks on the subject of this paper. Fluorescent particles were kindly provided by Dr. A. Imhof. This work is part of the research program of the Foundation for fundamental research on Matter (FOM) with financial support from the Netherlands Organization for Scientific Research (NWO).

[1] M. A. Tracey and R. Pecora, Macromolecules **25**, 337 (1992).
[2] O. A. Nehme, v. Johnson, and A. M. Donald, Macromolecules **22**, 4326 (1989).
[3] E. C. Cooper, P. Johnson, and A. M. Donald, Macromolecules **24**, 5380 (1991).
[4] N. Nemoto *et al.*, Macromolecules **18**, 2516 (1985).
[5] D. Gold, C. Onyenemezu, and W. G. Miller, Macromolecules **29**, 5710 (1996).
[6] T. F. Kosar and R. J. Phillips, AIChE. J. **41**, 701 (1995).
[7] T.-H. Lin and G. D. J. Phillies, Macromolecules **17**, 1686 (1984).
[8] P. S. Russo *et al.*, J. Colloid Interface Sci. **122**, 120 (1988).
[9] T. Yang and A. M. Jamieson, J. Colloid Interface Sci. **126**, 220 (1988).
[10] D. Gold, C. Onyenemezu, and W. G. Miller, Macromolecules **29**, 5700 (1996).
[11] M. A. Tracey, J. L. Garcia, and R. Pecora, Macromolecules **26**, 1862 (1993).
[12] W. Brown and R. Rymden, Macromolecules **21**, 840 (1988).
[13] X. Cao *et al.*, Biophys. J. **73**, 1932 (1997).
[14] D. N. Turner and F. R. Hallett, Biochim. Biophys. Acta **451**, 305 (1976).
[15] S. C. De Smedt *et al.*, Macromolecules **27**, 141 (1994).
[16] J. K. G. Dhont, *An Introduction to Dynamics of Colloids* (Elsevier, Amsterdam, 1996).
[17] G. D. J. Phillies *et al.*, J. Phys. Chem. **93**, 6219 (1989).
[18] G. D. J. Phillies *et al.*, Macromolecules **20**, 2280 (1987).
[19] G. S. Ullmann *et al.*, J. Phys. Chem. **89**, 692 (1985).
[20] W. Brown and R. Rymden, Macromolecules **20**, 2867 (1987).
[21] S. Gorti and B. R. Ware, J. Chem. Phys. **83**, 6449 (1985).
[22] K. Ullmann, G. S. Ullmann, and G. D. J. Phillies, J. Colloid Interface Sci. **105**, 315 (1985).
[23] Z. Zhou *et al.*, Macromolecules **27**, 1759 (1994).
[24] G. D. J. Phillies *et al.*, Macromolecules **26**, 6849 (1993).
[25] Z. Bu and P. S. Russo, Macromolecules **27**, 1187 (1994).
[26] D. Langevin and F. Rondelez, Polymer **19**, 875 (1978).
[27] T.-H. Lin and G. D. J. Phillies, J. Colloid Interface Sci. **100**, 82 (1984).
[28] S. C. De Smedt *et al.*, Macromolecules **30**, 4863 (1997).
[29] R. E. Cameron, M. A. Jalil, and A. M. Donald, Macromolecules **27**, 2708 (1994).
[30] I. H. Park, C. S. Johnson, Jr., and D. A. Gabriel, Macromolecules **23**, 1548 (1990).
[31] S. Matsukawa and I. Ando, Macromolecules **29**, 7136 (1996).
[32] G. D. J. Phillies *et al.*, J. Chem. Phys. **82**, 5242 (1985).
[33] G. D. J. Phillies, Macromolecules **19**, 2367 (1986).
[34] G. D. J. Phillies, Macromolecules **20**, 558 (1987).
[35] G. D. J. Phillies, J. Phys. Chem. **93**, 5029 (1989).
[36] G. D. J. Phillies and P. Peczak, Macromolecules **21**, 214 (1988).
[37] A. G. Ogston, B. N. Preston, and J. D. Wells, Proc. R. Soc. London, Ser. A **333**, 297 (1973).
[38] R. I. Cukier, Macromolecules **17**, 252 (1984).
[39] A. R. Altenberger, M. Tirrell, and J. S. Dahler, J. Chem. Phys. **84**, 5122 (1996).
[40] R. J. Philips, W. M. Deen, and J. F. Brady, AIChE. J. **35**, 1761 (1989).
[41] R. J. Philips, W. M. Deen, and J. F. Brady, J. Colloid Interface Sci. **139**, 363 (1990).
[42] P. A. Buining *et al.*, J. Am. Ceram. Soc. **74**, 1303 (1991).
[43] M. P. B. van Bruggen, Langmuir **14**, 2245 (1998).
[44] A. van Blaaderen and A. Vrij, Langmuir **8**, 2921 (1992).
[45] A. Imhof, Ph.D. thesis, University of Utrecht, 1996.
[46] W. Stöber, A. Fink, and E. Bohn, J. Colloid Interface Sci. **26**, 62 (1968).

[47] M. Doi and S. F. Edwards, *The Theory of Polymer Dynamics* (Clarendon, Oxford, 1988).
[48] T. Sato and A. Teramoto, Macromolecules **24**, 193 (1991).
[49] A. M. Wierenga and A. P. Philipse, J. Colloid Interface Sci. **180**, 360 (1996).
[50] A. M. Wierenga, Ph.D. thesis, University of Utrecht, 1997.
[51] A. Imhof *et al.*, J. Chem. Phys. **100**, 2170 (1994).
[52] A. van Blaaderen and J. G. K. Dhont, J. Chem. Phys. **96**, 4591 (1992).
[53] D. M. E. Thies-Weesie, Ph.D. thesis, University of Utrecht, 1995.
[54] Z. Dogic *et al.* (unpublished).
[55] W. Kuhn and H. Kuhn, Helv. Chim Acta **28**, 97 (1945).
[56] D. H. Berry and W. B. Russel, J. Fluid Mech. **180**, 475 (1987).
[57] M. M. Tirado, J. Chem. Phys. **81**, 2047 (1984).
[58] M. P. B. van Bruggen, H. N. W. Lekkerkerker, and J. K. G. Dhont, Phys. Rev. E **56**, 4394 (1997).
[59] G. H. Koenderink *et al.*, Langmuir **15**, 4693 (1999).
[60] A. P. Philipse and S. G. J. M. Kluijtmans, Physica A (to be published).
[61] C. N. Onyenemezu *et al.*, Macromolecules **26**, 3833 (1993).
[62] D. S. Clague and R. J. Philips, Phys. Fluids **8**, 1720 (1996).